Babol University Of Medical Sciences

IJMCM, Winter 2026, VOL 15, NO 1

International Journal of Molecular and Cellular Medicine

Journal homepage: www.ijmcmed.org

ORIGINAL ARTICLE

Combined application of Zinc and Iron nanoparticles with bacteriophage therapy against antibiotic-resistant *Staphylococcus aureus* biofilms

Ashkan Dirbaziyan[1], Mohammadreza Zolfaghari[1] *, Mohammad Soleimani[2], Ruhollah Mirjani[3], Seyed Soheil Aghaei[1]

1. Department of Microbiology, Qo.C., Islamic Azad University, Qom, Iran.
2. Department of Microbiology, Ti.t., AJA University of Medical Sciences, Tehran, Iran.
3. Department of Genetics and Advanced Technologies, Ti.t., AJA University of Medical Sciences, Tehran, Iran.

ARTICLE INFO

Received: 2025/05/28
Revised: 2026/01/2
Accepted: 2026/02/7

***Corresponding**:
Mohammadreza Zolfaghari
Address:
Department of Microbiology, Qo.C., Islamic Azad University, Qom, Iran
E-mail:
mo.zolfaghari123@iau.ir

ABSTRACT

This study investigated the combined antibacterial and anti-biofilm effects of zinc oxide nanoparticles, iron oxide nanoparticles, and a newly isolated bacteriophage, BacPhage-SAU27, against *Staphylococcus aureus* SAU27as a multidrug-resistant strain. The study aimed to evaluate the potential synergistic effects of phage–nanoparticle combinations in combating biofilm-related infections caused by multidrug-resistant *S. aureus*. *S. aureus* was cultured and evaluated for biofilm formation. BacPhage-SAU27 was isolated from wastewater using the double-layer agar method and characterized by plaque assays. The minimum inhibitory concentration of zinc oxide nanoparticles and iron oxide nanoparticles was determined individually and in combination, and BacPhage-SAU27 was added to assess interaction effects. Biofilm formation and destruction were analyzed using crystal violet staining and scanning electron microscopy, and the fractional inhibitory concentration index was calculated. The minimum inhibitory concentrations for zinc oxide nanoparticles and iron oxide nanoparticles were 120 µg/mL and 72 µg/mL, respectively. The combination of both nanoparticles reduced the minimum inhibitory concentration to 25 µg/mL. Adding BacPhage-SAU27 further reduced the minimum inhibitory concentration to 15 µg/mL for zinc oxide nanoparticles and 18 µg/mL for iron oxide nanoparticles and lowered the multiplicity of infection to 0.00001. BacPhage-SAU27 alone and in combination with nanoparticles significantly inhibited biofilm formation and caused biofilm destruction. Scanning electron microscopy confirmed damaged biofilm structures and complete bacterial clearance with the phage–nanoparticle combination. The combination of BacPhage-SAU27 with zinc oxide and iron oxide nanoparticles offers a promising strategy to combat *S. aureus* biofilms and may provide an alternative to antibiotic therapies.

Keywords: *Staphylococcus aureus*; Antibiotic-resistant bacteria; Phage; Iron and zinc nanoparticles.

Cite this article: Dirbaziyan A, et al. Combined application of Zinc and Iron nanoparticles with bacteriophage therapy against antibiotic-resistant Staphylococcus aureus biofilms. International Journal of Molecular and Cellular Medicine. 2026; 15 (1):1196-1215. DOI: 10.22088/IJMCM.BUMS.15.1.1196

[Downloaded from ijmcmed.org on 2026-11-08]

[DOI: 10.22088/IJMCM.BUMS.15.1.1196]

© The Author(s).
Publisher: Babol University of Medical Sciences
This work is published as an open access article distributed under the terms of the Creative Commons Attribution 4.0 License (http://creativecommons.org/licenses/by-nc/4). Non-commercial uses of the work are permitted, provided the original work is properly cited.

Introduction

Staphylococcus aureus is a well-known and clinically significant bacterium that can cause various infectious diseases in human and animal hosts via several modes of infection. A variety of illnesses are classified as human infections, including suppurative infections, meningitis, pneumonia, and pericarditis. Conversely, infections in animals might present as localized or systemic conditions such as septicemia, bovine mastitis, or avian arthritis (1, 2). Typically, the introduction of medical instruments into the body can cause a breach in the skin barriers. Resistance mechanisms against immunological responses and medications, biofilm formation on foreign objects significantly contributes to disease progression (3, 4). The global spread of multidrug-resistant lineages has greatly hindered treating *S. aureus* biofilm-associated infections (5, 6).

This situation necessitates the identification of new bacterial targets to develop innovative anti-infection strategies. To prevent harmful bacterial infections, one potentially proper technique is to utilize viruses that particularly target bacteria, known as phages or bacteriophages. Phages have been used to treat human bacterial infections since they were first identified (7). Phages are currently being studied as potential alternatives to antibiotics to help decrease the presence of pathogens on medical equipment (8). They reduce the likelihood of antibiotic cross-resistance by targeting receptors on bacterial cell envelopes and offering distinct modes of action (9). Phage therapy minimizes changes to the microbiome because off-target commensals have remarkable specificity, even down to subspecies levels, making them unlikely to become infected (10).

Besides, specific phages hold enzymes capable of depolymerizing polysaccharides, which allows them to break down bacterial biofilms (11). The development of complex defensive mechanisms against phage infections in *S. aureus* strains, has most likely limited the availability of phages for phage treatment. In the widely distributed laboratory strain RP62A, there are several components that provide resistance against phage infections. These include the type I restriction-modification system, eukaryotic-like serine/threonine kinase (Stk2), and type III-A clustered regularly interspaced short palindromic repeats (CRISPR)-Cas system (12, 13)

Using bacterial strains for cultures that are known to be sensitive to phages is highly contributory to better identification of a broader range of *S. aureus* phages (14). In addition, using nanoparticles has gained popularity as an alternative treatment for bacterial infections, replacing antibiotics. Nanoparticles use a distinct mechanism to target bacteria without the need to penetrate bacterial cells, thus establishing novel pathways (15).

Iron plays a vital part as a micronutrient for bacteria, participating in various biological processes such as energy metabolism and DNA synthesis (16). It also has a substantial effect on the pathogenicity of microorganisms. Iron primarily creates potent compounds with biomolecules such as heme within the host, resulting in an iron-deficient environment to which bacteria must adapt using a variety of iron acquisition mechanisms (17). Considering their remarkable antibacterial activity, affordability, simplicity of synthesis, and production scalability, zinc nanoparticles (ZnNPs) are appealing alternatives to conventional treatment methods. ZnNPs can potentially harm bacteria in two ways. Firstly, they interact electrostatically with bacterial cell walls, which can result in the breakdown of cell integrity. Secondly, they attach to the bacterial membrane and release zinc ions, causing mechanical damage and generating reactive oxygen species (ROS) (18, 19).

This study specifically investigates the synergistic effects of combining BacPhage-SAU27 with ZnONPs and IONPs to target biofilm-associated *S. aureus* infections. Unlike previous studies that focus on phages or nanoparticles individually, this research evaluates the combination of both approaches as a novel strategy to enhance antibacterial activity and biofilm disruption.

Methods

Sampling and isolation of *S. aureus* strains

Based on the code of ethics taken from the University of Central Florida, a total of 71 clinical isolates were collected from hospitalized patients. The isolates were systematically acquired from Milad, Imam Khomeini, and Imam Hossein Hospitals in Tehran between April 2022 and March 2023 as has been shown in Table S1 (see Supplementary Data). Specimens were collected using swabs and immediately transferred to the Microbiology Section of

[Downloaded from ijmcmed.org on 2026-11-08]

[DOI: 10.22088/IJMCM.BUMS.15.1.1196]

the ABCD Laboratory to maintain the integrity of the samples. The study included a review of all experiments conducted on the 71 clinical strains, as well as a control strain of *S. aureus* (ATCC 25923) obtained from the Iranian Pasteur Institute.

All samples were first incubated for 24 h at 37°C in blood agar (Merck, Germany). Conventional biochemical tests, including catalase, coagulase, mannitol fermentation, DNase, and oxidase tests, were performed under the standards of the American Society for Microbiology to identify the isolates according to their criteria.

To investigate *S. aureus* molecularly, primers were developed to target the coagulase gene (coa), a critical pathogenic factor was involved in host plasma coagulation. A product of 1050 base pairs (bp) was produced by the proposed primers, forward: 5'-TGCAGATGGATATTATTGGGG-3' and Reverse: 5'-GGTCTGTTTTGTTCCATTGTTG-3' (20). DNA extraction followed the E.Z.N.A.® Bacterial DNA Kit protocol, and subsequent nanodrop analysis confirmed the quality and quantity of the extracted DNA. The PCR (Master mix 2x Amplicon: 12.5 µL, Primer: 1 µL, DNA: 100 ng, water: up to 25 µL) followed a temperature protocol of 95°C; 30 s, 56°C; 20 s, 72°C; 40 s (30 cycles).

The bacterial strains used in the study included *Staphylococcus aureus* ATCC 25923, *S. aureus* S11, *S. aureus* S80, *S. aureus* 207, *S. aureus* 114, *S. aureus* S33, *Pseudomonas aeruginosa* ATCC 27853, *Salmonella enterica* ATCC 14028, *Streptococcus pneumoniae* ATCC 49619, and *Enterococcus faecalis* ATCC 29212.

Isolation of multiple drug resistance (MDR) strains

Multidrug resistance (MDR) is defined as the no susceptibility to at least one agent in three or more antimicrobial categories (21). To identify a suitable bacterial host for phage isolation, an antibiogram test was performed on clinical isolates to determine their resistance profiles against a panel of antibiotics. Antibiotic susceptibility was evaluated using the disk diffusion method, following the guidelines of the Clinical and Laboratory Standards Institute (CLSI). The tested antibiotics (Mast, England) included: azithromycin (15 µg), methicillin (5 µg), clindamycin (2 µg), tetracycline (30 µg), erythromycin (15 µg), ceftriaxone (10 µg), gentamicin (10 µg), nalidixic acid (25 µg), penicillin (1 µg), and nitrofurantoin (20 µg).

In accordance with current CLSI-endorsed phenotypic methods, cefoxitin disk diffusion was used as the preferred marker for detecting *mec*A-mediated methicillin resistance in *S. aureus*, owing to its higher sensitivity and specificity compared to oxacillin or methicillin (22). Regarding the inclusion of nalidixic acid and nitrofurantoin, while these antibiotics are primarily used for urinary tract infections, they were included to provide a broader antimicrobial susceptibility profile of the isolates (23). Although these antibiotics are not typically used for wound infections, their inclusion was intended to give a more comprehensive overview of the resistance patterns of the isolates.

After culturing the isolates on Mueller-Hinton agar, antibiotic discs were placed on the agar surface, and the plates were incubated at 37°C for 24 h. The diameters of the inhibition zones were then measured (24). The vancomycin susceptibility of *S. aureus* isolates was determined using the broth microdilution method according to CLSI guidelines. Briefly, bacterial suspensions adjusted to 0.5 McFarland standard were exposed to two-fold serial dilutions of vancomycin. MIC values were recorded after 18–24 hours of incubation at 37°C. Resistance was interpreted following CLSI breakpoints. Among the clinical isolates, the SAU27 strain—originally isolated from a patient sample—demonstrated resistance to nine different antibiotics and was thus selected as a representative MDR strain. Multidrug resistance (MDR) is defined as non-susceptible to ≥1 agent in >3 antimicrobial categories (25). Due to its high resistance profile, SAU27 was used as the host strain for subsequent bacteriophage isolation, purification, and further experimental analyses (21).

Bacteriophage isolation and purification

Wastewater samples were aseptically collected from Milad, Imam Khomeini, and Imam Hossein Hospitals in Tehran over one calendar year based on the following reference (26). Samples were promptly transported to the laboratory under sanitary conditions to ensure phage viability. After initial centrifugation at 6,000 × g for 10 min, the supernatant was filtered through a 0.22 µm membrane filter (Sartorius, Germany) to eliminate bacterial cells. To enrich bacteriophage populations, 10 mL of filtered wastewater was mixed with 10 mL of Luria-Bertani (LB) broth (Merck, Germany) and inoculated with the

[Downloaded from ijmcmed.org on 2026-11-08]

[DOI: 10.22088/IJMCM.BUMS.15.1.1196]

previously isolated *S. aureus* clinical strain SAU27 at a turbidity equivalent to 0.5 McFarland standard. The mixture was incubated at 37°C for 24 h with gentle shaking. Following incubation, the culture was centrifuged again at 6,000 × g for 10 min, and the supernatant was filtered using a 0.22 µm syringe filter to obtain phage-containing lysate.

Phage Detection and Plaque Assay

A double-layer agar method was employed to detect lytic bacteriophages (27). Briefly, 100 µL of the filtered lysate was mixed with 100 µL of SAU27 bacterial suspension (0.5 McFarland) and supplemented with one mM $CaCl_2$ (Sigma-Aldrich). The mixture was incubated at 37°C for 15 min to allow phage adsorption, then added to 3 mL of molten LB soft agar (0.7% w/v agar) maintained at 45°C. This overlay was poured onto pre-warmed LB agar plates and incubated at 37°C for 18–24 h. The appearance of clear plaques indicated the presence of lytic bacteriophages.

Phage purification and enumeration

Individual plaques were isolated using a sterile Pasteur pipette and suspended in 500 µL of SM buffer (100 mM NaCl, eight mM $MgSO_4$, 50 mM Tris-HCl, pH 7.5). The purification process was repeated through three successive rounds of the double-layer agar technique to ensure the isolation of a single phage type. The titer of the purified phage was determined by performing serial tenfold dilutions in SM buffer, followed by plaque assay. Plaque-forming units per milliliter (PFU/mL) were calculated using the formula:

$$\text{PFU/mL} = \frac{\text{Number of plaques counted}}{\text{Dilution factor} \times \text{Volume of sample plated (mL)}}$$

The isolated and purified bacteriophage was designated as Bacteriophage *S. aureus* 27 (BacPhage-SAU27) and used in further experiments (26).

Preparation of Bacterial Strain and Phage

Phage titre and MOI determination were carried out according to standard procedures described previously (14). The bacterial strain *S. aureus* SAU27, resistant to nine antibiotics, was cultured in LB medium at 37°C with shaking. Wastewater samples were used to isolate and concentrate BacPhage-SAU27. The plaque assay was employed to titrate the phage stock to a concentration of 2×10^8 PFU/mL. The multiplicity of infection (MOI) was calculated by using the ratio of infectious phage particles to bacterial cells. The optimal MOI for *S. aureus* SAU27 and BacPhage-SAU27 was determined based on these titrations.

Before phage exposure, *S. aureus* SAU27 was cultured to an optical density (OD600) of 0.6 in phosphate-buffered saline (PBS), equivalent to approximately 10^8 CFU/mL. The bacterial culture was then supplemented with BacPhage-SAU27 at various MOIs (MOI 1: 2×10^8 PFU/mL, MOI 0.1: 2×10^7 PFU/mL, MOI 0.01: 2×10^6 PFU/mL, MOI 0.001: 2×10^5 PFU/mL, MOI 0.0001: 2×10^4 PFU/mL, MOI 0.00001: 2×10^3 PFU/mL). Negative controls (LB medium only) and positive controls (*S. aureus* without phage) were included. The range of MOI values from 0.00001 to 1 was selected to evaluate phage efficacy under different bacterial-to-phage ratios. Lower MOIs (0.00001 to 0.001) mimic conditions with limited phages and high bacterial density, while higher MOIs (0.01 to 1) assess phage activity when phages are abundant. This approach helps to understand phage lysis efficiency and its interaction with nanoparticles across various infection scenarios.

The bacterial-phage mixture was incubated at 37°C for 15 minutes to allow for phage adsorption. After incubation, the mixture was centrifuged at 6,000 × g for 10 minutes, and the supernatant was discarded to remove unabsorbed phages. The pellet was washed twice with LB/PBS to ensure complete removal of free phages. The final bacterial pellet was resuspended in fresh PBS and incubated at 37°C.

Absorbance at 630 nm (OD600) was measured every 30 minutes to monitor bacterial growth and phage-mediated inhibition. At selected time points, serial dilutions were plated on LB agar to determine viable bacterial counts (CFU/mL). This ensured that changes in OD600 accurately reflected bacterial survival, rather than cell debris or lysis byproducts. The data from these experiments were used to identify the optimal MOI for BacPhage-SAU27 and to assess its lytic potential against *S. aureus* SAU27 based on a protocol as previously was reported (28).

One-step growth curve

A BacPhage-SAU27 suspension was added to LB broth containing *S. aureus* SAU27 at a concentration of 10^6 CFU/mL, with a MOI of 0.01. After 10 min of incubation at 37°C to allow for phage adsorption, the

[Downloaded from ijmcmed.org on 2026-11-08]

[DOI: 10.22088/IJMCM.BUMS.15.1.1196]

mixture was centrifuged at 10,000 × g for 5 min to separate unabsorbed (free) phages. The resulting bacterial pellet, which contained adsorbed phages, was washed once with sterile LB broth and then resuspended in 50 mL of fresh LB broth. Subsequently, 500 µL aliquots of the suspension were collected at 5-minute intervals for a total duration of 90 min. The double-layer agar method was used to determine BacPhage-SAU27 titers at each time point. Based on the resulting one-step growth curve, the latent period and burst size were calculated, as described previously (29), it is possible to determine the burst magnitude and latency duration more readily.

Bacteriophage Host Range

The phage was exposed to additional hosts besides its primary host (*S. aureus* isolated from patient SAU27) to assess its potential host range (prepared from Pasteur Institute Tehran, Iran). The plaques on the plates were examined for each bacterial strain using the two-layer agar technique (30).

Transmission electron microscopy (TEM)

The morphological features of BacPhage-SAU27 were examined using TEM. The phage suspension was immobilized on 400 mesh copper grids. The phages were immobilized and subsequently stained negatively with 2% phosphotungstic acid. A German-made Zeiss-EM10C-100 KV TEM was used for the imaging process (31).

Sodium dodecyl sulfate-polyacrylamide gel electrophoresis (SDS-PAGE) of structural proteins

The structural proteins of BacPhage-SAU27 were analyzed using the SDS-PAGE lamina technique. First, a 10% concentration separating gel was created by combining distilled water, bis-acrylamide (30%), 1.5 M Tris-base (pH 8.8), SDS (10%), ammonium persulfate (10%), and Tetramethylethylenediamine (TEMED). Next, distilled water, bis-acrylamide (30%), Tris-based 1M (pH6.8), SDS (10%), ammonium persulfate (10%), and TEMED were mixed to form a compression gel with a 5% concentration.

Subsequently, the gel was placed in a 1200 mL electrophoresis solution containing 0.1% SDS, 190 mM of glycine, and 25 mM of Tris base. Phage solutions (20 µL each) were added to the wells using a white sampler, and then boiled in 2X sample buffer for 5 min. The sample buffer contained SDS at 4%, 2-mercaptoethanol at 10%, glycerol at 20%, bromophenol at 0.004%, and Tris-HCl at 0.125 M. Furthermore, a pre-stained protein marker (PM2600) was included in one of the wells. The electrophoresis process began with an initial voltage of 80 and was subsequently raised to 120 (32).

Phage stability

The thermal stability of BacPhage-SAU27 was assessed by exposing isolated phage suspension to various temperatures, including 40°C, 50°C, 60°C, 70°C, and 80°C. At every temperature, samples were taken at 20, 40, and 60-minute intervals. The BacPhage-SAU27 suspension was further subjected to a pH range of 2 to 14, with sampling taking place at each pH point after 1, 2, and 3 hours, to ascertain phage stability. Furthermore, the sensitivity of the phage was evaluated by exposing the phage suspension to 26 µW/cm² of UV radiation, with samples being taken every 15 min (29).

Zinc oxide nanoparticles (ZnONPs) and iron oxide nanoparticles (IONPs)

ZnO and Fe_3O_4 nanoparticles used in this study were purchased from MSE PRO (USA) with stated purity > 99.9%. According to supplier's datasheet, ZnO NPs had average sizes of 30, 50 or 90 nm; Fe_3O_4 NPs had size range 50–100 nm. Since we used commercial powders, no further physicochemical characterization (e.g. PDI, zeta potential, TEM) was performed — this is acknowledged as a limitation.

Evaluation of phage stability to nanoparticles

A suspension of BacPhage-SAU27 was prepared and exposed to different concentrations of IONPs and ZnONPs. The nanoparticles (0.065, 10, and 20 mg/mL) were added to the phage suspension at a concentration of 2×10^8 PFU/mL. The mixtures were incubated at 37°C for 12, 24, and 36 h to evaluate the direct effects of the nanoparticles on phage stability.

Following incubation, the phage suspension was mixed with a bacterial culture of *S. aureus* SAU27, which had been grown to a concentration of 10^6 CFU/mL. The mixture was incubated for 15 min at 37°C, allowing the phage to adsorb to the bacterial cells. To determine the phage titer, a double-layer agar method was employed. The phage-bacteria mixture was poured onto LB agar plates and incubated at 37°C for 24 h. Plaques were counted, and the phage titer was

[Downloaded from ijmcmed.org on 2026-11-08]

[DOI: 10.22088/IJMCM.BUMS.15.1.1196]

determined based on the plaque-forming units (PFU) observed (33).

Assessment of ZnONPs, IONPs, and BacPhage-SAU27 Effects on *S. aureus* SAU27 Using the MIC Test

The effects of ZnONPs, IONPs, and their combination with BacPhage-SAU27 on the bacterial strain *S. aureus* SAU27 were evaluated using the Minimum Inhibitory Concentration (MIC) test. The primary objectives were to determine the lowest concentrations of phage and nanoparticles required to inhibit bacterial growth and to assess any potential synergistic effects between the two agents.

Each well of a 96-well microplate received 100 µL of Mueller-Hinton cation-adjusted broth (MHB). Varying concentrations of ZnONPs (240, 120, 60, 30, 15, 7.5, 3.75, and 1.875 µg/mL) and their equivalent concentrations of IONPs (144, 72, 36, 18, 9, 4.5, 2.25 µg/mL) were added to the wells. Additionally, combinations of both nanoparticles at the same concentrations were tested. All nanoparticle concentrations originally expressed in ppm were converted to µg/mL based on the equivalence of 1 ppm = 1 µg/mL for aqueous solutions.

To evaluate potential synergistic interactions between the nanoparticles and BacPhage-SAU27, the Fractional Inhibitory Concentration (FIC) Index was calculated. The FIC Index is used to quantify the interaction between two agents, with values less than 1 indicating a synergistic effect. The individual MIC values for the nanoparticles and phage were first determined, followed by the calculation of the FIC Index for each combination.

Different concentrations of BacPhage-SAU27 (0.01, 0.001, 0.0001, and 0.00001) were added to the wells, followed by 100 µL of an isolated bacterial suspension of *S. aureus* SAU27 (at 10^6 PFU/mL). The positive control contained bacteria without phage, while the negative control included only the culture medium. The microplate was incubated at 37°C for 24 hours to allow bacterial growth and phage activity.

After incubation, bacterial growth was assessed by measuring absorbance at 630 nm. The lowest concentration at which no bacterial growth was observed, based on absorbance readings, was considered the MIC for each treatment. Serial dilutions of the cultures were also plated on LB agar to determine viable bacterial counts (CFU/mL), ensuring that changes in absorbance reflected actual bacterial survival rather than cell debris or lysis byproducts. The wells were then investigated to look for signs of bacterial development. MIC was defined as the lowest substance concentration that could inhibit bacterial growth (33).

Investigation of biofilm formation and biofilm inhibition ability

To investigate the biofilm formation ability of *S. aureus* SAU27 and its inhibition by ZnONPs, IONPs, and BacPhage-SAU27, the following procedure was followed. First, a bacterial suspension of *S. aureus* SAU27 was prepared to achieve a turbidity of 0.5 McFarland. Two hundred µL of the suspension was added to each well of a 96-well microplate containing Mueller-Hinton broth, a suitable medium for biofilm formation by *S. aureus*. The microplate was incubated at 37°C for 24 hours to allow biofilm formation.

After the incubation period, the biofilm formed in each well was assessed as a control, with no treatment applied, to determine the bacteria's natural biofilm formation. Following this, ZnONPs and IONPs were added at concentrations two and four times their respective Minimum Inhibitory Concentrations (MIC) to the wells.Because MIC values are determined for planktonic cells, and biofilm-associated cells commonly exhibit higher tolerance and reduced antimicrobial susceptibility due to matrix-associated diffusion barriers and physiological heterogeneity, nanoparticles were additionally tested at 2× and 4× minimum inhibitory concentration to evaluate a standardized supra-minimum inhibitory concentration dose–response and to assess partial versus near-complete biofilm inhibition/elimination, as performed in prior antibiofilm studies.

Accordingly, in our study we tested ZnONPs and IONPs at 2×MIC and 4×MIC to evaluate both partial and full biofilm inhibition, in line with previous reports using such elevated doses (34). BacPhage-SAU27 was then introduced in triplicate to the wells, at a multiplicity of infection (MOI) of 0.0001, to evaluate its impact on biofilm inhibition. The microplate was incubated at 37°C for another 24 hours. After the second Biofilm formation was classified into the following categories (35):

Negative biofilm formation, Poor biofilm formation, Moderate biofilm formation, Strong biofilm formation; these cutoff values were established based on control

[Downloaded from ijmcmed.org on 2026-11-08]

[DOI: 10.22088/IJMCM.BUMS.15.1.1196]

data and are supported by relevant literature to accurately differentiate the biofilm-producing capacities of the tested samples. To evaluate the effects of nanoparticles and BacPhage-SAU27 on biofilm formation, biofilm inhibition was assessed by comparing treated wells with untreated controls. The degree of biofilm inhibition was calculated as the percentage reduction relative to the control (36). This provided the relative biofilm formation as a percentage. Detailed raw and processed data, including triplicate measurements for biofilm quantification, are provided in Table S2 and Table S3 (see Supplementary Data).

Evaluation of the Efficacy of IONPs and BacPhage-SAU27 in Biofilm Elimination

To assess the biofilm elimination efficacy of IONPs and BacPhage-SAU27, biofilms were initially formed using *S. aureus* SAU27 as described previously. Following biofilm formation, varying concentrations of ZnONPs and IONPs, specifically at MIC, 2×MIC, and 4×MIC, were introduced to the wells. Given the increased resistance of biofilm- embedded bacterial cells compared to their planktonic counterparts, it is a common practice in antibiofilm research to apply nanoparticle concentrations above the MIC determined for planktonic bacteria. Nanoparticles can penetrate the biofilm matrix more effectively at higher doses, disrupting extracellular polymeric substances (EPS) and killing embedded bacteria. BacPhage-SAU27 was added at a multiplicity of infection (MOI) of 0.0001 to evaluate its impact on biofilm inhibition.

The microplate was incubated at 37°C for 24 hours. After this incubation, biofilm destruction was assessed by crystal violet staining and classified by biofilm type. To quantify biofilm reduction, the percentage of biofilm reduction was calculated. A significant reduction in biofilm formation indicated effective biofilm destruction.

Investigation of Biofilm Destruction by Scanning Electron Microscopy (SEM)

To assess biofilm destruction, biofilms were initially formed on 12-mm round glass coverslips in a 24-well microplate using *S. aureus* SAU27 as previously described. After 24 h of biofilm formation, the coverslips were washed twice with sterile PBS to remove any non-adherent bacteria. Subsequently, the biofilm samples were treated with ZnONPs and IONPs at their MIC concentrations, and BacPhage-SAU27 was applied at a MOI of 0.0001. The samples were incubated for an additional 24 h at 37°C. Following the incubation period, the samples were rewashed with PBS to remove any unbound nanoparticles and phages. The biofilm samples were then fixed in 2.5% glutaraldehyde at 4°C for 2 h to preserve the biofilm structure. After fixation, the samples were dehydrated through a series of ethanol concentrations (30%, 50%, 70%, 90%, and 100%) for 10 min at each step. The samples were then air-dried and coated with a thin layer of gold to improve conductivity.

Finally, the samples were examined under a scanning electron microscope (SEM) at a suitable magnification (e.g., 5000x) to observe the biofilm structure and evaluate the effects of ZnONPs, IONPs, and BacPhage-SAU27 on biofilm destruction.

Statistical analysis

All experiments were performed in triplicate (n= 3). Data were expressed as mean ± standard deviation (SD). Statistical analyses were conducted using one-way ANOVA followed by Tukey's post-hoc test to compare multiple groups. Student's t-test was used for pairwise comparisons. A p-value of less than 0.05 was considered statistically significant. All analyses were performed in GraphPad Prism ver. 9 (GraphPad Software, USA). For MIC and biofilm assays, comparisons were performed against untreated controls unless stated otherwise.

Results

***S. aureus* isolates**

Using the standards set by the American Society for Microbiology, 67 isolates were verified from 71 clinical specimens. These findings are included in the article's appendix section as supplemental information. 82.1% of these isolates were resistant to methicillin, and over 95% were resistant to tetracycline and penicillin.

Furthermore, 79.1% showed resistance to ceftriaxone and nalidixic acid, while 35.8% displayed resistance to clindamycin and azithromycin. Vancomycin resistance, determined via MIC testing, was 20.9%. Conversely, 91 % of the isolates were susceptible to gentamicin. Table 1 provides the antimicrobial susceptibility patterns of *S. aureus* isolates against nine antibiotics with chi-square analysis.

[Downloaded from ijmcmed.org on 2026-11-08]

[DOI: 10.22088/IJMCM.BUMS.15.1.1196]

Table 1. Antibiotic susceptibility profile of *Staphylococcus aureus* isolates (n= 67) with chi-square analysis.

Antibiotic	S n(%)	I n(%)	R n(%)	Total	χ^2	p-value
Methicillin	12 (17.9)	0 (0.0)	55 (82.1)	67	74.90	<0.001
Tetracycline	3 (4.5)	0 (0.0)	64 (95.5)	67	116.81	<0.001
Penicillin	3 (4.5)	0 (0.0)	64 (95.5)	67	116.81	<0.001
Ceftriaxone	10 (14.9)	4 (6.0)	53 (79.1)	67	63.97	<0.001
Nalidixic Acid	10 (14.9)	4 (6.0)	53 (79.1)	67	63.97	<0.001
Clindamycin	14 (20.9)	29 (43.3)	24 (35.8)	67	5.22	>0.05
Azithromycin	14 (20.9)	29 (43.3)	24 (35.8)	67	5.22	>0.05
Vancomycin (MIC)	43 (64.2)	10 (14.9)	14 (20.9)	67	29.04	<0.001
Gentamycin	61 (91.0)	0 (0.0)	6 (9.0)	67	101.22	<0.001

S = Susceptible; I = Intermediate; R = Resistant. Chi-square (χ^2) test with df=2 comparing observed distribution against equal distribution. Significance: $p<0.05$.

Bacteriophage isolation and phage PFU titer determination

Sixteen strains were selected as hosts for bacteriophages from isolated strains (SAU7, SAU15, SAU27, SAU30, SAU43, and SAU56). The coagulase gene was present in these bacteria, which were also resistant to penicillin, tetracycline, methicillin, nalidixic acid, azithromycin, clindamycin, and vancomycin, among other nine drugs.

BacPhage-SAU27 successfully induced plaque formation on three patient strains, with the standard strain of *S. aureus* (ATCC 25923) serving as a positive control. SAU27, which had the highest number of plaques, was later identified as the bacteriophage host. When SAU27 was cultured with BacPhage-SAU27 and the BacPhage-SAU27 two-layer agar test was performed, the estimated phage titer was approximately 10^5 PFU/ml.

The effect of BacPhage-SAU27 on the lysis of SAU27

Figure 1 illustrates the effect of BacPhage-SAU27-induced lysis on SAU27. This graph was generated by analyzing the absorption kinetics of samples taken at various time points. The positive control bacterial culture medium underwent growth analysis for 15 h. Nevertheless, the culture media used as the negative control, without any bacteria, exhibited no growth and remained unaltered. After three hours, the absorption levels at MOI: 1 showed a declining trend, indicating bacterial lysis. After 10 h, the absorption levels exhibited a downward trend at MOI: 0.00001, suggesting bacterial lysis. These results indicate that increasing the MOI leads to a more effective phage-mediated bacterial lysis.

BacPhage-SAU27 Host Specificity (quantitative EOP)

The formation of plaque was attributed to the isolated bacteriophage BacPhage-SAU27, which selectively targeted antibiotic-resistant *S. aureus* from patient SAU27 and other strains of the same bacterial type. The results showed that the phage had no significant impact on the gram-negative bacteria (*Pseudomonas* and *Salmonella*) or the gram-positive bacteria (*S. pneumoniae* and *E. faecalis*). The efficiency of plating (EOP) values for the bacterial strains was as follows: 1 for *S. aureus* (SAU27), 0.74 for *S. aureus* S11, 0.16 for *S. aureus* S80, 0.55 for *S. aureus* 207, 0.45 for *S. aureus* 114, 0.32 for *S. aureus* S33, and 0 for *Pseudomonas aeruginosa*, *Salmonella enterica*, *Streptococcus pneumoniae*, and *Enterococcus faecalis*. Therefore, no lysis was observed in any of these instances.

One-step growth curve and burst size

When SAU27 bacteria are treated with BacPhage-SAU27, the resulting one-stage growth curve (Figure 2) displays a latent period of 30 min and burst size of approximately 820 PFU per infected cell.

BacPhage-SAU27 Morphology and family identification

Phages can be taxonomically categorized based on their physical characteristics, and the majority fall into one of three families: Myoviridae, Siphoviridae, or

[Downloaded from ijmcmed.org on 2026-11-08]

[DOI: 10.22088/IJMCM.BUMS.15.1.1196]

Podoviridae (37). Our phage is classified under Myoviridae based on TEM analysis. Double-stranded (ds) DNA is commonly found in the genomes of Myoviridae phages (38). A hexagonal head and tail configuration are exhibited by the phage, as illustrated in Figure 3.

The object's diameter and length are approximately 80 to 170 nm.

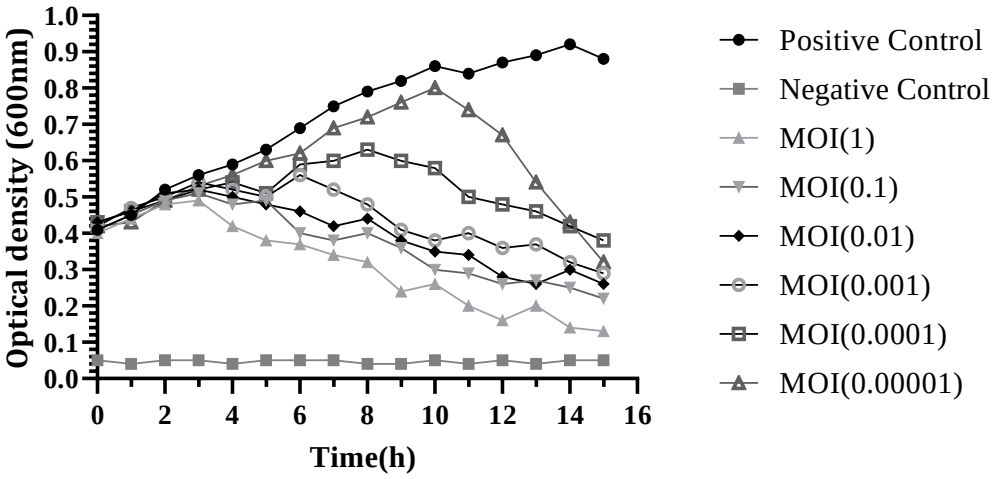


Figure 1. Effect of lysing BacPhage-SAU27 at different MOIs on SAU27. An absence of bacterial growth was observed in the negative control, while the positive control exhibited an increase in bacterial growth. When varying the MOIs, there was an initial growth followed by a subsequent decrease in bacterial growth. As the MOI increased, there was a corresponding increase in the rate of phage lysis on bacteria.

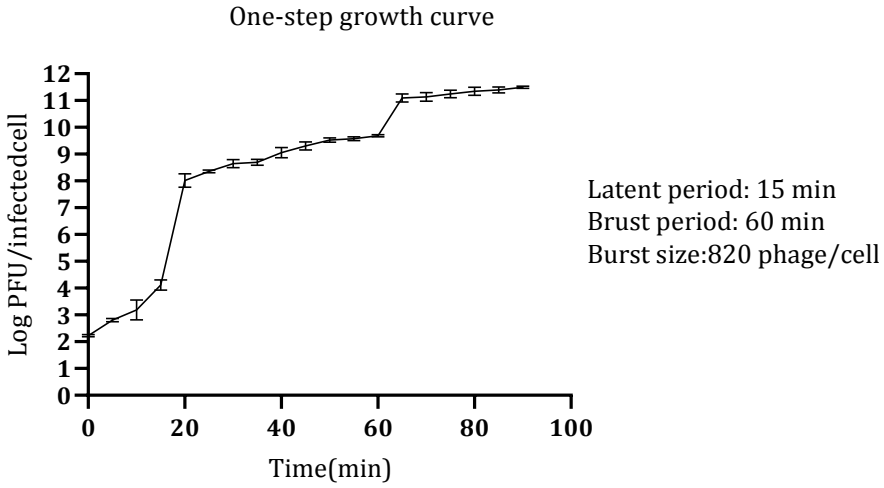


Figure 2. One-step growth curve of BacPhage-SAU27. The graph shows the latent period of 15 minutes, a burst period of 60 minutes, and a burst size of approximately 820 phages per infected cell. A direct correlation is observed between the timing of the lysis and the burst size, indicating efficient phage replication and bacterial lysis during the growth cycle.

[Downloaded from ijmcmed.org on 2026-11-08]

[DOI: 10.22088/IJMCM.BUMS.15.1.1196]

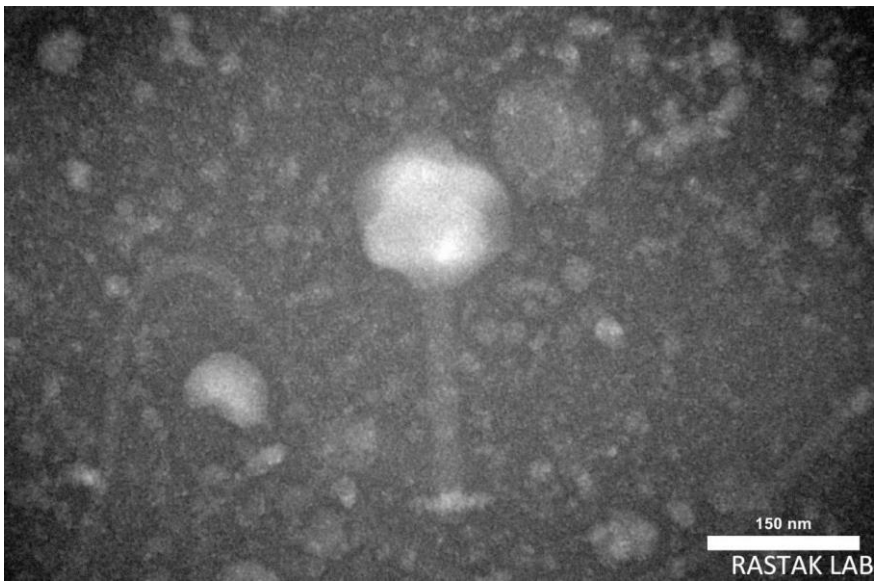


Figure 3. TEM image of BacPhage-SAU27 showing its characteristic morphology with a hexagonal head and a long tail. The scale bar represents 150 nm. This micrograph confirms the typical structure of a Myoviridae bacteriophage.

SDS-PAGE of BacPhage-SAU27 structural proteins

Figure 4 presents an SDS-PAGE image depicting the isolated proteins of BacPhage-SAU27. As illustrated in Figure 4, the discernible protein bands range in size from approximately 15 kDa to over 245 kDa, as determined by comparison with the protein ladder.

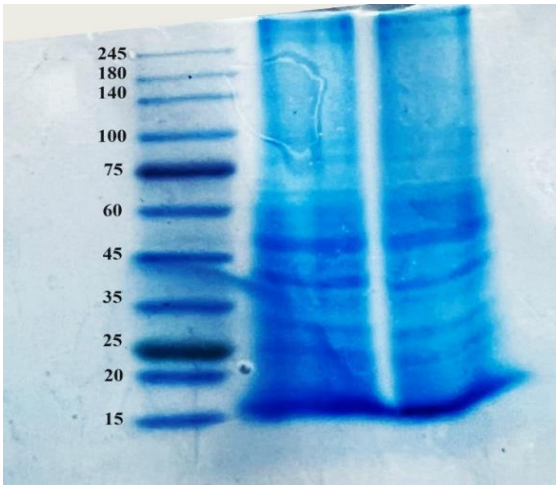


Figure 4. SDS-PAGE analysis of BacPhage-SAU27 structural proteins. The gel shows distinct protein bands, with molecular weights ranging from approximately 15 kDa to over 245 kDa, as indicated by the protein ladder. This profile suggests a complex composition of structural proteins, characteristic of the BacPhage-SAU27.

BacPhage-SAU27 Stability

The thermal stability graph of BacPhage-SAU27 illustrated its resilience across various temperatures (Figure 5-A). At a temperature of 40°C, the phage shows stability; even at 50°C, it continues to demonstrate relatively strong stability. However, within the first five minutes, stability drops significantly between 60°C and 70°C and vanishes entirely at 80°C.

Following a three-hour incubation, the pH stability graph demonstrates (Figure 5-B) robust stability within pH levels ranging from 7 to 11. However, there is a noticeable decline over time when the pH falls below seven or exceeds 11. The UV sensitivity graph (Figure 5-C) shows remarkable stability in the first fifteen minutes of exposure. But after that, the phage stability progressively decreases. The results from the resistance to nanoparticle diagram (Figure 5-D) suggest that ZnONPs are superior to in terms of phage resistance reduction. As the concentrations of nanoparticles and the duration of phage exposure increase, the level of phage resistance decreases.

[Downloaded from ijmcmed.org on 2026-11-08]

[DOI: 10.22088/IJMCM.BUMS.15.1.1196]

The thermal stability diagram illustrates the resistance of BacPhage-SAU27 at various temperatures. The phage showed relatively good stability up to 50°C. The pH stability chart displays the resistance of phage at different pH levels, demonstrating its ability to endure pH levels ranging from 7 to 11. UV sensitivity graph illustrates the phage's response to UV rays, indicating that it can withstand exposure for a maximum of 15 min. The resistance of phage to two nanoparticles is depicted in the nanoparticle resistance diagram. It illustrates that the resistance decreases as the concentration of nanoparticles and the time of phage effect increase.

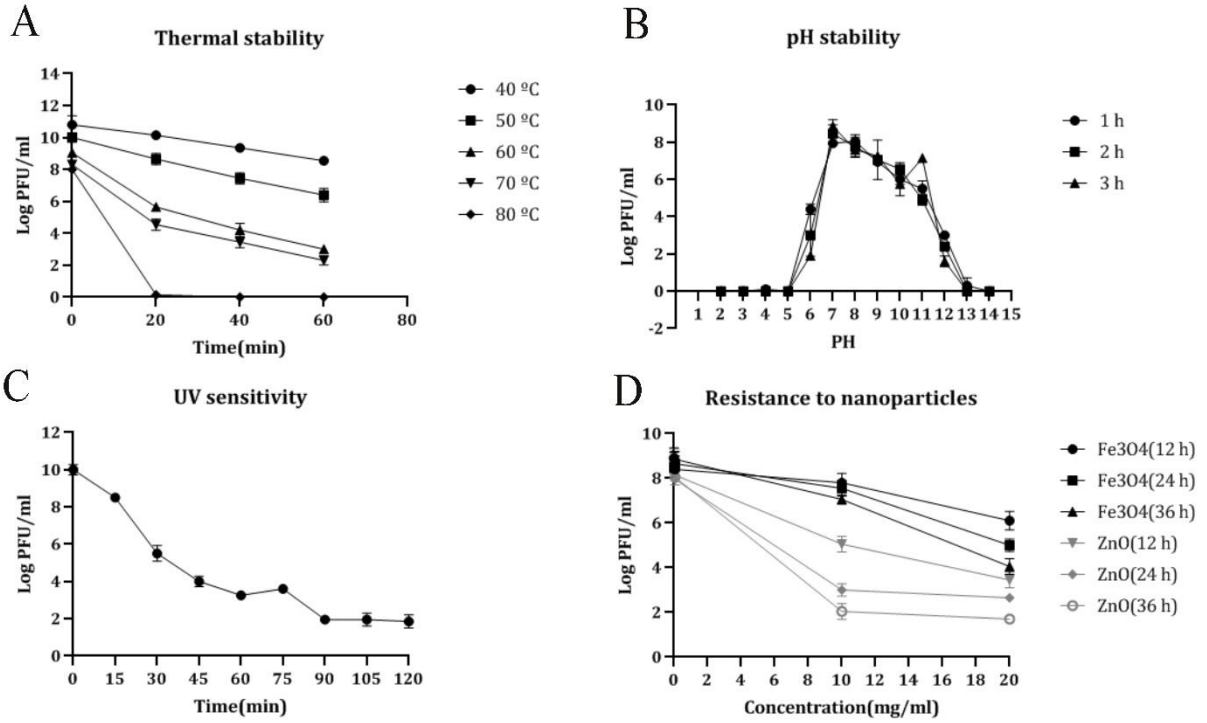


Figure 5. Stability of BacPhage-SAU27 under various environmental conditions. (A) The thermal stability panel demonstrates that BacPhage-SAU27 maintains relatively good stability at temperatures up to 50°C, with a marked decline in activity at higher temperatures (60°C and above). (B) The pH stability chart shows the phage's resilience across a broad pH range, with optimal stability observed between pH 7 and pH 11. Phage activity significantly decreased when exposed to extreme acidic or alkaline conditions. (C) The UV sensitivity graph illustrates the phage's vulnerability to UV irradiation, with a sharp reduction in activity after 15 minutes of exposure. (D) Finally, the resistance to nanoparticles graph indicates that BacPhage-SAU27's stability is inversely correlated with nanoparticle concentration and exposure time, as both Fe_3O_4 and ZnO nanoparticles progressively reduce phage activity over time and concentration.

MIC, biofilm formation and additive antibacterial effect of ZnONPs, IONPs and BacPhage-SAU27

ZnONPs alone showed an MIC of 120 µg/mL against SAU27 strain, while IONPs alone had an MIC of 72 µg/mL. The simultaneous use of both nanoparticles resulted in a significant reduction in the MIC to 25 µg/mL. The calculated fractional inhibitory concentration (FIC) index for this combination was 0.56. Since the FIC index for the phage–nanoparticle combination was 0.56, the interaction is classified as additive rather than synergistic.

BacPhage-SAU27 alone was effective in inhibiting SAU27 at an MOI of 0.001. The addition of IONPs reduced the MIC to 36 µg/mL and the MOI to 0.0001. Similarly, in the presence of ZnONPs, the MIC reached 30 µg/mL at an MOI of 0.0001. The combination of phage with both nanoparticles resulted in a further reduction in MIC (Fe_3O_4 : 18 µg/mL; ZnO: 15 µg/mL) and a significant decrease in MOI to 0.00001.

[Downloaded from ijmcmed.org on 2026-11-08]

[DOI: 10.22088/IJMCM.BUMS.15.1.1196]

These findings indicate the additive effect of the combination of phage and nanoparticles in increasing antibacterial activity against SAU27.

The results in Table 2 show that the presence of iron nanoparticles had little effect on the ability of SAU27 bacteria to form biofilms and the possibility of bacterial biofilm development was maintained in their presence. Bacteria formed weak biofilms at MICs close to ZnONPs, while no biofilms were observed at concentrations of two and four times the MIC. In the combination of the two nanoparticles, moderate biofilms were observed at MICs and no biofilm formation was observed at two and four times the MICs, similar to the single nanoparticle. At an MOI of 0.0001, bacteria formed moderate biofilms under the influence of phage.

When phage was used in combination with IONPs at MIC, little biofilm was formed, but at concentrations of two and four times the MIC, no biofilm was formed. The combination of phage with ZnONPs or with both nanoparticles completely inhibited biofilm formation. Findings on the efficacy of nanoparticles and BacPhage-SAU27 in destroying SAU27 biofilm are presented in Table 3.

Iron oxide nanoparticles, phage, and their combination alone or together had no significant effect on biofilm removal. However, ZnONPs alone or in combination with phage caused significant biofilm destruction. Also, the simultaneous use of ZnONPs and IONPs along with phage had a similar effect on biofilm eradication

Further examination with SEM showed that in the control sample (Figure 6), bacteria and the possibility of biofilm formation were present, while the bacterial population decreased in the samples treated with IONPs and ZnONPs together with phage. The sample treated with ZnONPs alone and phage significantly reduced the bacterial population. However, in the phage sample together with nanoparticles, no bacteria were observed.

The SEM images were consistent with the results of the biofilm formation experiments. Biofilm formation was significantly reduced by ZnONPs at all concentrations. ZnONPs at MIC reduced biofilm to 13% of the untreated control ($p < 0.001$), while 2× and 4× MIC almost completely inhibited biofilm formation ($p < 0.001$). IONPs alone did not significantly reduce biofilm formation at MIC ($p = 0.09$), but a mild reduction was observed at 2× MIC ($p = 0.04$). Phage treatment alone reduced biofilm to 50% of the control ($p = 0.003$). The combination of ZnONPs and phage showed the greatest reduction ($p < 0.001$).

Moreover, ZnONPs significantly disrupted preformed biofilms with an 86% reduction ($p < 0.001$). IONPs alone produced a small, non-significant reduction ($p = 0.06$). Phage alone significantly reduced biofilm ($p = 0.002$).

The ZnONP + phage combination produced the highest biofilm destruction (91%, $p < 0.001$). IONP + phage treatment showed moderate but significant reduction ($p = 0.01$).

Table 2. Biofilm formation under the influence of different concentrations of nanoparticles and BacPhage-SAU27.

Treatment Group	MIC, MOI	2×MIC, MOI	4×MIC, MOI
	Biofilm Type	Biofilm Type	Biofilm Type
Fe_3O_4	Strong	Strong	Strong
ZnO	Poor	Negative	Negative
Phage	Moderate	Moderate	Moderate
ZnO + Fe_3O_4	Moderate	Negative	Negative
Fe_3O_4 + Phage	Poor	Negative	Negative
ZnO + Phage	Negative	Negative	Negative
Fe_3O_4 + ZnO + Phage	Negative	Negative	Negative

Table 3. Effect of different concentrations of nanoparticles and BacPhage-SAU27 on biofilm destruction.

Treatment	Biofilm Type	Biofilm Degradation (%)
Fe_3O_4 (4×MIC, MOI)	Strong	88.0%

[Downloaded from ijmcmed.org on 2026-11-08]

[DOI: 10.22088/IJMCM.BUMS.15.1.1196]

Treatment	Biofilm Type	Biofilm Degradation (%)
Fe_3O_4 (2×MIC, MOI)	Moderate	82.2%
Fe_3O_4 (MIC, MOI)	Moderate	79.4%
ZnO (4×MIC, MOI)	Strong	70.3%
ZnO (2×MIC, MOI)	Strong	73.3%
ZnO (MIC, MOI)	Strong	70.5%
Phage (4×MIC, MOI)	Moderate	86.1%
Phage (2×MIC, MOI)	Moderate	76.1%
Phage (MIC, MOI)	Strong	68.2%
ZnO + Fe_3O_4 (4×MIC, MOI)	Strong	61.3%
ZnO + Fe_3O_4 (2×MIC, MOI)	Strong	38.4%
ZnO + Fe_3O_4 (MIC, MOI)	Strong	73.1%
Fe_3O_4 + Phage (4×MIC, MOI)	Moderate	78.8%
Fe_3O_4 + Phage (2×MIC, MOI)	Moderate	76.8%
Fe_3O_4 + Phage (MIC, MOI)	Moderate	85.6%
ZnO + Phage (4×MIC, MOI)	Moderate	77.0%
ZnO + Phage (2×MIC, MOI)	Moderate	82.4%
ZnO + Phage (MIC, MOI)	Moderate	76.2%

*Biofilm type classification: Negative, Poor, Moderate, Strong based on crystal violet staining intensity.

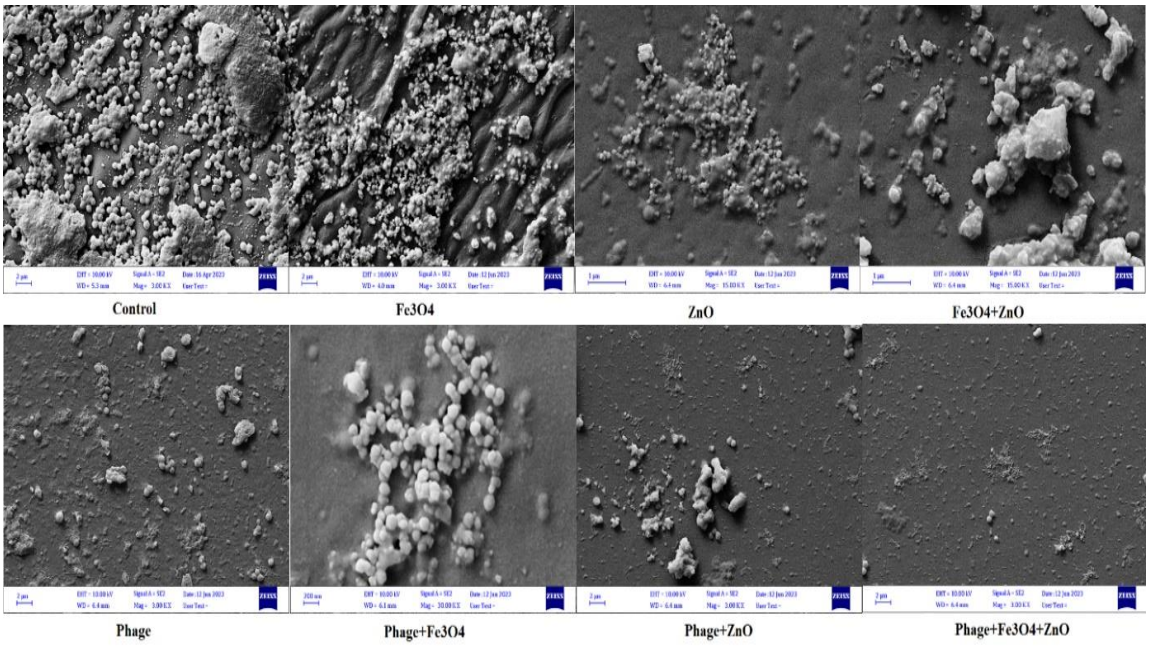


Figure 6. Scanning Electron Microscopy (SEM) imaging illustrating the effects of various nanoparticles and BacPhage-SAU27 on biofilm formation by *S. aureus* SAU27. The images show the biofilm structure under different treatment conditions: the control group (untreated) exhibits a dense and intact biofilm, while treatments with Fe_3O_4 nanoparticles, ZnONPs, and their combinations with BacPhage-SAU27 demonstrate varying levels of biofilm disruption. The most significant inhibition of biofilm formation was observed in the ZnONPs-treated samples. BacPhage-SAU27, particularly when combined with ZnONPs, showed marked destruction of biofilm structures, with a reduction in bacterial populations and biofilm matrix degradation. The scale bar at the bottom represents 1 µm.

[Downloaded from ijmcmed.org on 2026-11-08]

[DOI: 10.22088/IJMCM.BUMS.15.1.1196]

Discussion

In this study, we investigated the combined effect of a host-directed bacteriophage (BacPhage-SAU27) and ZnONPs and IONPs on multidrug-resistant *S. aureus* and biofilm formation. The innovative aspects of this study include the use of specific phage against antibiotic-resistant strains, which allows for precise targeting of problematic bacteria; the evaluation of the combined effect of phage and nanoparticles by carefully examining MIC, MOI, and biofilm inhibition, which indicate additive or synergistic interactions between these factors; and the provision of a mechanistic analysis based on ROS production by ZnONPs and Fenton reaction by Fe(hinok)3, which helps to better understand the combined effect of phage and nanoparticles.

By providing novel and targeted approaches to combat antibiotic-resistant *S. aureus* and persistent biofilms, this study could provide an effective alternative to traditional therapies and open new avenues for future research in the application of phage and nanoparticles in chronic infections. Our findings showed that BacPhage-SAU27 selectively infects antibiotic-resistant strains of *S. aureus* and no significant lytic effect was observed on Gram-negative or some other Gram-positive bacteria. This host-specific property is consistent with previous studies and suggests that this phage could serve as a targeted tool in the treatment of resistant infections. Our EOP data also confirm the limited host range of the phage, increasing its importance in clinical application (39, 40). The phage titer was 10^5 PFU/mL after bacteriophage-inoculated bacterial culture and the two-layer agar test were performed. The life cycle of our phage closely resembled that of other Staphylococcus phages from Myoviridae family, such as Stau2 (NC_030933) (100 PFU/cell) and IME-SA1 (NC_047729) (80 PFU/cell) (41, 42).

One-step growth curve analysis showed that BacPhage-SAU27 has a short incubation period (15 min) and a burst period of about 60 min, and the number of phage produced per infected cell was estimated to be about 820 PFU/cell. This relatively high burst size and short incubation period indicate the rapid ability of the phage to reduce bacterial populations. Comparison with similar studies shows slight differences in burst size and incubation period, which could be due to differences in host cell density, environmental conditions, or bacterial genetic differences. These features are particularly valuable in the treatment of chronic infections with low bacterial densities, as the phage can replicate rapidly and inhibit bacteria in the early stages of the infection cycle.

Besides, the results indicate that a higher MOI is associated with a greater degree of phage-mediated bacterial lysis. This pattern aligns with the findings of Wang et al., who demonstrated that phage SA2 displayed bacteriolytic activity in laboratory settings. Their analysis revealed that a significant percentage of bacteria died after 24 h owing to phage SA2 lysis across all MOIs; the rate of absorption reduced over the first few hours (3-7 h), depending on MOI values.

Therefore, a more rapid decrease in absorbance at 600 nm was observed with higher MOI values. For instance, at MOI 1, the uptake began to decline approximately two hours after the co-incubation started (43). Besides, Zhang's study found that cultures of *S. aureus* (ATCC 6538) infected with phage JS25 (MOI 1) showed a significant decrease in absorbance (OD600) compared to uninfected cultures after 2 to 7 h. However, in the initial three hours of incubation, the strain culture showed a gradual increase in absorbance (OD600) in the absence of any phage infection (MOI 0) (44). In the analysis of the one-stage growth curve, it was observed that the isolated phage exhibited a latent period of 15 min and a burst duration of 60 min when exposed to *S. aureus* from the patient.

Moreover, the burst size measured 820 PFU/infected cells. In a study by Han et al. (35), comparative experiments were conducted to examine the latent period and burst size of the *S. phage* SAH-1. The results showed that the latent period was 20 min, and the burst size was 100 PFU/cell (45). Phases SA (30 min, 1000 phages) and MSA6 (15 min, 23 PFU/cell) were found to have similar characteristics (46). Longer burst sizes combined with shorter latent durations are usually regarded as favorable. However, longer latent periods may be preferred in specific conditions, such as when the host bacterial cell density is low (47). This work highlights the potential of Staphylococcus phage for therapeutic applications in chronic types of *S. aureus* bovine mastitis. These types of mastitis are typically characterized by low bacterial density (usually fewer than 10^4 PFU/mL), making this phage a promising option (48). However, further in

[Downloaded from ijmcmed.org on 2026-11-08]

[DOI: 10.22088/IJMCM.BUMS.15.1.1196]

vivo investigations are needed to determine the efficacy of the isolated phages.

The SDS-PAGE of isolated phage proteins showed bands of various sizes, ranging from approximately 15 kDa to over 245 kDa when compared to the protein ladder. In addition, the SDS-PAGE profiling revealed the affinity of our phage for Myoviridae phages. Based on previous studies, our phage seems to contain at least five structural proteins that are comparable to the MSA6 protein (49). In addition, research has demonstrated that phage K is highly effective in preventing biofilm formation and reducing bacterial colonization on materials utilized in central venous catheters (50). Phage stability measurements showed a significant decrease in viability at 80°C, with almost complete loss of viability. After three hours of incubation, the pH stability graph exhibited relatively strong stability within the pH range of 7–11. Over time, however, significant reductions in phage stability were observed at pH levels below 7 and above 11. The UV sensitivity graph demonstrated excellent stability during the initial 15 min. However, the phage's stability gradually diminished as the exposure duration increased.

As regards biofilm formation, bacteria near ZnONPs showed a weak biofilm at the MIC. No biofilm was observed at two and four times the MIC. When ZnONPs and IONPs were used in combination, the bacterium showed a slight biofilm formation at the MIC. At an MOI of 0.0001, the bacterium exhibited signs of a moderate biofilm. However, a minimal biofilm or no biofilm was observed when the phage was combined with nanoparticles. Thus, using ZnONPs, either on their own or in conjunction with the phage, resulted in a moderate level of biofilm removal. Nevertheless, the use of IONPs and the phage, either alone or in conjunction, did not have any significant impact on the elimination of biofilms.

Similarly, when the phage was used in combination with ZnONPs and IONPs, there was a modest reduction in biofilm. The research conducted by Abdul Sattar et al. provides support for our findings, as it demonstrates the synergistic efficacy of ecologically friendly ZnONPs generated from bacteriophage and *Ocimum basilicum* extract in reducing harmful bacteria. Specifically, bacteriophage ZCSE6 exhibits significant anti-pathogenic bacteriolytic action. An absorption peak at 370 nm is observed in the UV-Vis spectrum, while TEM images reveal the presence of irregular particles ranging in size from 10 to 25 nm. Furthermore, ZnONPs showed the ability to alter biofilms in *Staphylococcus sciuri* and exhibit antibacterial activity against Salmonella enterica when combined with phage ZCSE6 (51).

ZnO's antibacterial action is thought to be mediated via the extensively investigated and well-known ROS pathway. ROS, including highly reactive ionic species and free radicals, may cause cellular damage by triggering oxidative stress processes (52, 53). Oxidative stress occurs when there is an imbalance between the amounts of ROS produced and their reducing equivalents (54). Notably, ZnO releases electrons when exposed to UV or visible light (55).

Besides, there is an increasing tendency toward higher concentrations of ROS species when ZnONP concentrations increase. A study by Raghupati et al investigated the impact of ZnO on bacteria when exposed to UV light. Remarkably, the live cells of *S. aureus* were eliminated after a 30-minute exposure to UV radiation. This observation of activity in the presence of UV radiation highlights ROS's important role in antibacterial activity.

The accumulation of ZnONPs on the cell surface is greatly affected by the ionization of carboxylic, phosphate, and amino groups, resulting in a negative charge on the cell.

The study conducted by Abeydeera et al. highlights the crucial role of iron in the survival and growth of various organisms, including harmful bacteria. The Fenton reaction contradicts the biological significance of iron. This process is facilitated by iron and can lead to cell death caused by ROS when iron absorption is heightened. Abeydeera explains that iron-hinokitiol, or Fe(hinok)3, is a neutral Fe(III) complex that occurs naturally in combination with the metal chelator hinokitiol, which is a lipophilic and aromatic tropolone derivative. It is essential to observe that this lipophilic Fe(III) complex has the extraordinary ability to cross cellular membranes and deliver iron to eukaryotic cells. This property has been consistently observed in *S. aureus* bacterial cells.

Moreover, Fe^{3+} in Fe(hinok)3 does not serve as a potent Fenton catalyst. When Fe(III) enters bacterial cells, it reduces to Fe(II), resulting in the release of iron from the hinokitiol ligand molecules. This can be attributed to the fact that Fe(II) shows a substantially lower binding constant to the O-donating atoms of the Lewis acid in hinokitiol. Consequently, Fe(II) acts as a

[Downloaded from ijmcmed.org on 2026-11-08]

[DOI: 10.22088/IJMCM.BUMS.15.1.1196]

softer Lewis acid compared to Fe(III). Abeydeera's measurements of intracellular ROS production provide strong evidence for the reduction of Fe(III) to Fe (II). This reduction allows Fe(II) to donate an electron to H_2O_2, resulting in the generation of hydroxyl radicals through the Fenton reaction.

In addition to previously reported findings, our work shows a more significant antibiofilm effect of the nanoparticles and phage combination. It is noteworthy that the scientific literature lacks a precise mechanism describing how phages and nanoparticles collaborate to benefit this bacterium. Therefore, more research is advised into the mechanisms underlying the interaction with *S. aureus*.

SDS-PAGE and TEM studies revealed that BacPhage-SAU27 has at least five structural proteins and belongs to the Myoviridae family. These findings are consistent with previous studies and indicate that the protein structure of the phage plays an important role in its stability and efficacy. Evaluation of phage stability under different conditions of temperature, pH, and UV irradiation showed that the phage was stable in the range of 40–60°C and pH 6–9, but a significant decrease in activity was observed under extreme conditions. These results highlight the importance of choosing appropriate storage conditions and clinical application.

Analysis of the effect of nanoparticles and phage on biofilm showed that ZnONPs, either alone or in combination with phage, have a significant ability to reduce biofilm formation, while IONPs have a more limited effect. Combining nanoparticles with phage provides a slight additive effect. The difference in the effects of ZnONPs and IONPs is likely related to their mechanism of action: ZnONPs damage bacteria and reduce biofilm by producing ROS and inducing oxidative stress to cell membranes and components; whereas Fe3+ in IONPs has a strong antibacterial effect only under specific conditions and by activating the Fenton reaction. SEM images showed that the combination of phage and nanoparticles reduced bacterial populations and damaged cell membranes, which was consistent with the reduction of biofilm formation and the destruction of biofilm structure.

One of the key points of this study is the combined effect of phage and nanoparticles. The data show that the simultaneous use of ZnONPs and BacPhage-SAU27 leads to a more significant reduction in MIC and biofilm formation than the use of either agent alone. These findings are consistent with previous studies that have reported synergistic or additive effects between nanoparticles and phages, suggesting that the combination of these two agents could serve as an effective strategy to combat resistant bacteria (56, 57). However, the exact mechanism of interaction between phage and nanoparticles is still not fully understood and requires further studies, especially in in vivo environments. In terms of molecular mechanisms, data indicate that ROS plays a key role in the antibacterial effect of ZnONPs, generating reactive oxygen species, causing membrane damage and lipid peroxidation. Also, Fe (hinok)3 reduces Fe(III) to Fe(II) and activates the Fenton reaction, leading to the generation of hydroxyl radicals and increased intracellular toxicity. These mechanisms, together with the simultaneous effect of phage, are likely to lead to a reduction in bacterial population and inhibition of biofilm (58). Overall, the findings of this study suggest that BacPhage-SAU27 and ZnONPs, especially in combination, have high potential to inhibit *S. aureus* and reduce biofilm formation. These effects, combined with the targeting capabilities of phage and the mechanistic effects of nanoparticles, could provide a promising approach for the treatment of antibiotic-resistant infections. Further in vivo studies and molecular pathway investigation are recommended to better understand the molecular interactions and efficacy in clinical settings.

Based on the results of this study, although BacPhage-SAU27 was able to specifically target and exert significant lytic effects on antibiotic-resistant *S. aureus* strains, the impact of specific resistance mechanisms on the efficacy of the phage-nanoparticle combination has not been fully explored. It is likely that resistance to bacteriophages in *S. aureus* may involve mechanisms such as restriction-modification systems and CRISPR-Cas systems, which can reduce phage efficiency.

Additionally, bacterial resistance to nanoparticles may result from specific features of the bacterial cell membrane or the presence of surface molecules, such as protective proteins, which can interfere with nanoparticle interactions. The results in this study showed that the combination of ZnONPs and BacPhage-SAU27 was particularly effective in reducing biofilm formation and enhancing antibacterial effects. However, the exact role of specific resistance mechanisms on the efficacy of this combination

[Downloaded from ijmcmed.org on 2026-11-08]

[DOI: 10.22088/IJMCM.BUMS.15.1.1196]

therapy remains an area for further investigation. To better understand how *S. aureus* resistance characteristics influence the phage-nanoparticle interaction, more detailed studies focusing on the genetic and molecular aspects of resistance are recommended.

The limitations of this study include the lack of in vivo evaluation of the combined phage and nanoparticle therapy. In vivo experiments are crucial for assessing the safety, pharmacodynamics, and clinical efficacy of this therapeutic combination, ensuring its potential for clinical application in hospital settings. Additionally, the study does not fully characterize the nanoparticles used. While the size and source of the nanoparticles are mentioned, detailed physicochemical properties such as zeta potential, surface charge, and morphology are not provided. This information would enhance the understanding of nanoparticle behavior and their interaction with bacteria and phages. Furthermore, no genomic analysis (WGS) was performed to identify the genetic features of the phages. Whole genome sequencing (WGS) could help in precisely identifying the phage genes, including those related to resistance, molecular characteristics, and biofilm degradation capabilities.

Such analysis could offer deeper insights into the mechanisms of action of both phages and nanoparticles against *S. aureus*. This study provides compelling evidence regarding the therapeutic potential of a combined approach utilizing metal ions (iron and zinc) and a newly isolated bacteriophage against the multidrug-resistant pathogen *S. aureus*. Given the escalating threat posed by antibiotic-resistant *S. aureus* strains, this research explores viable alternatives to conventional antibiotic therapies. The findings demonstrate that the synergistic interaction between zinc and iron ions, coupled with BacPhage-SAU27, significantly inhibits the growth, proliferation, and biofilm formation of *S. aureus*.

This combination approach targets multiple bacterial vulnerabilities, thereby reducing the likelihood of resistance development. Importantly, the phage used in this study exhibits high host specificity, targeting *S. aureus* while sparing beneficial commensal microbiota, which underscores the precision of phage therapy as an alternative to broad-spectrum antibiotics.

While these results are promising, further in vivo investigations are warranted to assess the safety, pharmacodynamics, and long-term efficacy of this phage-nanoparticle combination in clinical settings. Such studies are crucial for determining its potential as a viable treatment modality for *S. aureus*-associated infections, particularly those involving biofilm formation, which are notoriously difficult to treat with conventional antimicrobial agents.

Acknowledgements

This study was conducted with financial support provided by the Department of Microbiology, Qom Branch, Islamic Azad University, Qom, Iran.

Funding

This study was supported in part by the Department of Microbiology, Qom Branch, Islamic Azad University, Qom, Iran. The experimental protocols were established in accordance with the Declaration of Helsinki.

The studies involving human participants were reviewed and approved by the Ethics Committee of the Qo.C., Islamic Azad University (reference number: IR.IAU.QOM.REC.1402.013). Written informed consent was obtained from all participants prior to their inclusion in the study.

References

1. Haag AF, Fitzgerald JR, Penadés JR. Staphylococcus aureus in Animals. Microbiol Spectrum. 2019;7(3):10.1128/microbiolspec.gpp3-0060-2019.
2. Touaitia R, Mairi A, Ibrahim NA, et al. Staphylococcus aureus: A Review of the Pathogenesis and Virulence Mechanisms. Antibiotics. 2025;14(5):470.
3. Wu H, Moser C, Wang H-Z, et al. Strategies for combating bacterial biofilm infections. Int J Oral Sci. 2015;7(1):1-7.
4. Jan Z, Norouzi Taheri H, Danesh A. Optimizing Production Conditions of a Caspian Sea Actinomycete Exhibiting Promising Antibacterial Activity Against Clinically-important Pathogens Using the Two-Factor Interaction/Minimum Run Resolution IV Method. Int J Mol Med. 2025:0-.
5. Lee JY, Monk IR, Gon╟alves da Silva A, et al. Global spread of three multidrug-resistant lineages of Staphylococcus epidermidis. Nat Microbiol. 2018;3(10):1175-85.

[Downloaded from ijmcmed.org on 2026-11-08]

[DOI: 10.22088/IJMCM.BUMS.15.1.1196]

6. Yal▒ד▫n S. Candida albicans Impact on the Progression, Morphology, and Cellular Integrity of Biofilm Formation on the Surfaces of Implants; Current Knowledge and Future Perspectives. Int J Mol Med. 2025:0-.
7. Abedon ST, Kuhl SJ, Blasdel BG, et al. Phage treatment of human infections. Bacteriophage. 2011;1(2):66-85.
8. Cui L, Watanabe S, Miyanaga K, et al. A comprehensive review on phage therapy and phage-based drug development. Antibiotics. 2024;13(9):870.
9. Loc-Carrillo C, Abedon ST. Pros and cons of phage therapy. Bacteriophage. 2011;1(2):111-4.
10. Koskella B, Meaden S. Understanding bacteriophage specificity in natural microbial communities. Viruses. 2013;5(3):806-23.
11. Topka-Bielecka G, Dydecka A, Necel A, et al. Bacteriophage-derived depolymerases against bacterial biofilm. Antibiotics. 2021;10(2):175.
12. Depardieu F, Didier J-P, Bernheim A, et al. A eukaryotic-like serine/threonine kinase protects staphylococci against phages. Cell Host Microbe. 2016;20(4):471-81.
13. Moller AG, Lindsay JA, Read TD. Determinants of phage host range in Staphylococcus species. Appl Environ Microbiol. 2019;85(11):e00209-19.
14. Hyman P. Phages for phage therapy: isolation, characterization, and host range breadth. Pharmaceuticals. 2019;12(1):35.
15. Wang L, Hu C, Shao L. The antimicrobial activity of nanoparticles: present situation and prospects for the future. Int J Nanomedicine. 2017;12:1227-49.
16. Dev S, Babitt JL. Overview of iron metabolism in health and disease. Hemodial Int. 2017;21:S6-S20.
17. Eijkelkamp BA, Hassan KA, Paulsen IT, et al. Investigation of the human pathogen Acinetobacter baumannii under iron limiting conditions. BMC genomics. 2011;12:1-14.
18. Ko▒ッodziejczak-Radzimska A, Jesionowski T. Zinc oxide¬タヤfrom synthesis to application: a review. Materials. 2014;7(4):2833-81.
19. Pradeev Raj K, Sadaiyandi K, Kennedy A, et al. Influence of Mg doping on ZnO nanoparticles for enhanced photocatalytic evaluation and antibacterial analysis. Nanoscale Res Lett. 2018;13:1-13.
20. Effendi MH, Hisyam MAM, Hastutiek P, et al. Detection of coagulase gene in Staphylococcus aureus from several dairy farms in East Java, Indonesia, by polymerase chain reaction. Vet World. 2019;12(1):68.
21. Chew CH, Yeo CC, Che Hamzah AM, et al. Multidrug-resistant methicillin-resistant Staphylococcus aureus associated with hospitalized newborn infants. Diagnostics. 2023;13(6):1050.
22. Broekema NM, Van TT, Monson TA, et al. Comparison of cefoxitin and oxacillin disk diffusion methods for detection of mecA-mediated resistance in Staphylococcus aureus in a large-scale study. J Clin Microbiol. 2009;47(1):217-9.
23. Keys T, editor Antimicrobials commonly used for urinary tract infection: sulfonamides, trimethoprim-sulfamethoxazole, nitrofurantoin, nalidixic acid. Mayo Clinic Proceedings; 1977.
24. Humphries RM, Ambler J, Mitchell SL, et al. CLSI methods development and standardization working group best practices for evaluation of antimicrobial susceptibility tests. J Clin Microbiol. 2018;56(4):10.1128/jcm. 01934-17.
25. Magiorakos A-P, Srinivasan A, Carey RB, et al. Multidrug-resistant, extensively drug-resistant and pandrug-resistant bacteria: an international expert proposal for interim standard definitions for acquired resistance. Clin Microbiol Infect. 2012;18(3):268-81.
26. Samir S, El-Far A, Okasha H, et al. Isolation and characterization of lytic bacteriophages from sewage at an egyptian tertiary care hospital against methicillin-resistant Staphylococcus aureus clinical isolates. Saudi J Biol Sci. 2022;29(5):3097-106.
27. Ács N, Gambino M, Brøndsted L. Bacteriophage enumeration and detection methods. Front Microbiol. 2020;11:594868.
28. Egido JE, Toner-Bartelds C, Costa AR, et al. Monitoring phage-induced lysis of gram-negatives in real time using a fluorescent DNA dye. Sci Rep. 2023;13(1):856.
29. Jiang Y, Xu Q, Jiang L, et al. Isolation and Characterization of a Lytic Staphylococcus aureus Phage WV against Staphylococcus aureus Biofilm. Intervirology. 2021;64(4):169-77.
30. Jensen KC, Hair BB, Wienclaw TM, et al. Isolation and Host Range of Bacteriophage with Lytic

[Downloaded from ijmcmed.org on 2026-11-08]

[DOI: 10.22088/IJMCM.BUMS.15.1.1196]

Activity against Methicillin-Resistant Staphylococcus aureus and Potential Use as a Fomite Decontaminant. PLoS One. 2015;10(7):e0131714.
31. Aprea G, D¬ßAngelo A, Prencipe V, et al. Bacteriophage Morphological Characterization by Using Transmission Electron Microscopy. Journal of Life Sciences. 2015;10.
32. Yubuki N, Edgcomb VP, Bernhard JM, et al. Ultrastructure and molecular phylogeny of Calkinsia aureus: cellular identity of a novel clade of deep-sea euglenozoans with epibiotic bacteria. BMC Microbiol. 2009;9:1-22.
33. Ahiwale S, Bankar A, Tagunde S, et al. A bacteriophage mediated gold nanoparticles synthesis and their anti-biofilm activity. Indian J Microbiol. 2017;57:188-94.
34. Mohanta Y, Chakrabartty I, Mishra A, et al. Nanotechnology in combating biofilm: a smart and promising therapeutic strategy. Front Microbiol 13: 1028086. 2023.
35. Kamimura R, Kanematsu H, Ogawa A, et al. Quantitative analyses of biofilm by using crystal violet staining and optical reflection. Materials. 2022;15(19):6727.
36. Elsayed A, Safwat A, Abdelsattar AS, et al. The antibacterial and biofilm inhibition activity of encapsulated silver nanoparticles in emulsions and its synergistic effect with E. coli bacteriophage. Inorg Nano-Met Chem. 2023;53(6):549-59.
37. Deghorain M, Van Melderen L. The Staphylococci phages family: an overview. Viruses. 2012;4(12):3316-35.
38. Comeau AM, Tremblay D, Moineau S, et al. Phage morphology recapitulates phylogeny: the comparative genomics of a new group of myoviruses. PLoS One. 2012;7(7):e40102.
39. Moller AG, Winston K, Ji S, et al. Genes influencing phage host range in Staphylococcus aureus on a species-wide scale. Msphere. 2021;6(1):10.1128/msphere. 01263-20.
40. Krusche J, Beck C, Lehmann E, et al. Characterization and host range prediction of Staphylococcus aureus phages through receptor-binding protein analysis. Cell Rep. 2025;44(3).
41. Hsieh S-E, Lo H-H, Chen S-T, et al. Wide host range and strong lytic activity of Staphylococcus aureus lytic phage Stau2. Appl Environ Microbiol. 2011;77(3):756-61.
42. Fan J, Zeng Z, Mai K, et al. Preliminary treatment of bovine mastitis caused by Staphylococcus aureus, with trx-SA1, recombinant endolysin of S. aureus bacteriophage IME-SA1. Vet Microbiol. 2016;191:65-71.
43. Wang J, Zhao F, Sun H, et al. Isolation and characterization of the Staphylococcus aureus bacteriophage vB_SauS_SA2. AIMS Microbiol 5: 285¬ß307. 2019.
44. Zhang L, Bao H, Wei C, et al. Characterization and partial genomic analysis of a lytic Myoviridae bacteriophage against Staphylococcus aureus isolated from dairy cows with mastitis in Mid-east of China. Virus Genes. 2015;50:111-7.
45. Han JE, Kim JH, Hwang SY, et al. Isolation and characterization of a Myoviridae bacteriophage against Staphylococcus aureus isolated from dairy cows with mastitis. Res Vet Sci. 2013;95(2):758-63.
46. Hamza A, Perveen S, Abbas Z, et al. The lytic SA phage demonstrate bactericidal activity against mastitis causing Staphylococcus aureus. Open Life Sci. 2016;11(1):39-45.
47. Dennehy JJ, Abedon ST. Bacteriophage ecology. Bacteriophages. 2021:253-94.
48. Nagasawa Y, Kiku Y, Sugawara K, et al. Rapid Staphylococcus aureus detection from clinical mastitis milk by colloidal gold nanoparticle-based immunochromatographic strips. Front Vet Sci. 2020;6:504.
49. Kwiatek M, Parasion S, Mizak L, et al. Characterization of a bacteriophage, isolated from a cow with mastitis, that is lytic against Staphylococcus aureus strains. Arch Virol. 2012;157:225-34.
50. Lungren MP, Christensen D, Kankotia R, et al. Bacteriophage K for reduction of Staphylococcus aureus biofilm on central venous catheter material. Bacteriophage. 2013;3(4):e26825.
51. Abdelsattar A, Mohammed W, Mohamed S, et al. Utilization of Ocimum basilicum extracts for zinc oxide nanoparticles synthesis and their antibacterial activity after a novel combination with phage. Mater Lett. 2021;309:131344.
52. Jiang M, Zhang J, Qian L, et al. Moz forms an autoregulatory feedback loop with mir-223 in aml and monocyte/macrophage development. Iscience. 2019;11:189-204.

[Downloaded from ijmcmed.org on 2026-11-08]

[DOI: 10.22088/IJMCM.BUMS.15.1.1196]

53. Chen H, Liu C, Chen D, et al. Bacteria-targeting conjugates based on antimicrobial peptide for bacteria diagnosis and therapy. Mol Pharm. 2015;12(7):2505-16.
54. Rodrigo R, Libuy M, Feliǂ F, et al. Molecular basis of cardioprotective effect of antioxidant vitamins in myocardial infarction. Biomed Res Int. 2013;2013(1):437613.
55. Raghupathi KR, Koodali RT, Manna AC. Size-dependent bacterial growth inhibition and mechanism of antibacterial activity of zinc oxide nanoparticles. Langmuir. 2011;27(7):4020-8.
56. Alipour-Khezri E, Moqadami A, Barzegar A, et al. Bacteriophages and Green Synthesized Zinc Oxide Nanoparticles in Combination Are Efficient against Biofilm Formation of Pseudomonas aeruginosa. Viruses. 2024;16(6):897.
57. Abdelsattar AS, Nofal R, Makky S, et al. The synergistic effect of biosynthesized silver nanoparticles and phage zcse2 as a novel approach to combat multidrug-resistant salmonella enterica. Antibiotics. 2021;10(6):678.
58. Abeydeera N, Yu B, Pant BD, et al. Harnessing the toxicity of dysregulated iron uptake for killing Staphylococcus aureus: reality or mirage? Biomaterials Sci. 2022;10(2):474-84.

[Downloaded from ijmcmed.org on 2026-11-08]

[DOI: 10.22088/IJMCM.BUMS.15.1.1196]